

Application of the independent molecule model to elucidate the dynamics of structure I methane hydrate: A second report

Shuzo Yoshioki *

Yatsushiro National College of Technology, Yatsushiro 866-8501, Japan

Received 19 October 2007; received in revised form 13 January 2008; accepted 23 January 2008

Available online 5 February 2008

Abstract

Two model systems of methane hydrate are constructed. One has a small cage surrounded by 12 large cages. The other has a large cage surrounded by four small cages and ten large cages. Three different H-bonding network patterns between waters are formed, and three random configurations of methane in each cage are chosen. A new method called the surface water fixed model is presented in which the energy minimum conformations for both model systems are preserved close to the X-ray crystallized structure. With normal mode analysis, we calculated frequencies of 2916.6 cm^{-1} for a small cage at a centre, 2915.9 cm^{-1} not at a centre, and 2911.7 cm^{-1} for a large cage at a centre, and 2911.3 cm^{-1} not at a centre. These frequencies are in moderate agreement with the corresponding Raman spectra, though not adequate. With our new method, however, it should be possible to improve agreement with the Raman spectra, if a model system vastly larger than the present model systems were constructed.

© 2008 Published by Elsevier Inc.

Keywords: Methane hydrate; Structure I methane hydrate; Dynamics; Vibrational frequency; Independent molecule model; Raman spectrum; Hydrogen bond; Bond stretching mode; Thermal ellipsoid

1. Introduction

In our earlier paper on the independent molecule model [1], we demonstrated the dynamical vibrations of a methane as a guest molecule in ice-like hydrogen bonded cages. For modelling methane hydrate, we picked a dodecahedra, formed by 12 pentagons designated 5^{12} (the small cage), and a tetrakaidecahedra, formed by 12 pentagons and 2 hexagons designated $5^{12}6^2$ (the large cage) [2,3]. These cages are in contact, and each holds one methane. Raman spectroscopy has exhibited the C–H stretch (A_1 mode) frequency ν_1 of hydrated methanes at 2915 cm^{-1} for the 5^{12} cage and 2905 cm^{-1} for the $5^{12}6^2$ cage [4–6]. These values are lower than the frequency of 2916.5 cm^{-1} in gaseous methane. In this earlier paper, the theory led to 2915.4 cm^{-1} for the 5^{12} cage, and 2901.9 cm^{-1} for the $5^{12}6^2$ cage. The frequency in the $5^{12}6^2$ cage is shifted downward compared to the one in 5^{12} , and the frequencies in both cages

are shifted downward compared with the frequency in gas. This shows that our results are in reasonable agreement with observed Raman spectra. To reach these results, it was necessary to include the cubic anharmonic terms in addition to the harmonic terms in the potential energy calculation on methane [7,8], and further to include the hydrogen bonding (H-bonding) energy between methane hydrogen and water oxygen. For this H-bonding strength, we used 75% of the strength of the H-bonding potential energy between waters.

Our main purpose of the present article is to extend the two cages model system (a small cage and a large cage) used in our previous study to larger model systems, and to investigate whether we can produce the observed Raman spectra using the energy parameters adopted in the previous work.

In Section 2, the method of the independent molecule model (independent MM) and the potential energy E for methane hydrate are briefly described. See Ref. [1] for the details. In Section 3, model systems adopted are represented. The results are given in Section 4. Discussion and conclusion are in Section 5. Finally, the formulation of the Hessian matrix necessary to do energy minimization and normal mode

* Tel.: +81 965 53 1309; fax: +81 965 53 1319.

E-mail address: yoshioki@as.yatsushiro-nct.ac.jp.

analysis is given in Appendix A of Supplementary material in electronic form.

2. Independent molecule model

2.1. Variables in the independent molecule model

The independent MM was devised to elucidate the dynamical structure of internal motions and rigid-body motions of each molecule in a multi-molecule system. The essential point of the independent MM is to separate the motions of each molecule in the system into the rigid-body motion (with six degrees of freedom) and the internal motions. The variables describing movements as a rigid body are a translational vector and Eulerian angles specifying position and orientation of each molecule. The variables describing internal movements within methane are four bond lengths and six bond angles, while two bond lengths and one bond angle are chosen for water molecules.

2.2. Total potential energy E of methane hydrate

The total potential energy E for methane hydrate is briefly described as a sum of five energies as follows (for the details see Ref. [1]):

$$E = E_{\text{wat}} + E_{\text{wat-wat}} + E_{\text{met}} + E_{\text{met-met}} + E_{\text{met-wat}} \quad (1)$$

The first energy E_{wat} is an intramolecular interaction of water and is expressed as:

$$E_{\text{wat}} = \frac{1}{2} \sum_{\text{waters}} \sum_{v,\mu=1}^3 K_{v\mu} (\rho w_v^k - \rho w_{v,0}) (\rho w_\mu^k - \rho w_{\mu,0}) \quad (2)$$

The second energy $E_{\text{wat-wat}}$ is an intermolecular interaction between waters:

$$\begin{aligned} E_{\text{wat-wat}} = & \sum_{\text{pairs}} \frac{1}{4\pi\epsilon_0} \frac{q_i q_j}{r_{ij}} + \sum_{\text{pairs}} \left\{ \epsilon \left(\frac{r_0}{r_{ij}} \right)^{12} - 2\epsilon \left(\frac{r_0}{r_{ij}} \right)^6 \right\} \\ & + \sum_{\text{H-bonds}} \left\{ \epsilon \left(\frac{r_0}{r_{\text{HX}}} \right)^{12} - 2\epsilon \left(\frac{r_0}{r_{\text{HX}}} \right)^{10} \right\} \end{aligned} \quad (3)$$

The third energy E_{met} is an intramolecular interaction of methane and is expressed as below:

$$E_{\text{met}} = \sum_{\text{methanes}} \{V^{(2)} + V^{(3)}\} \quad (4)$$

where $V^{(2)}$ describes a harmonic potential energy and $V^{(3)}$ is the cubic anharmonic potential energy.

The fourth energy $E_{\text{met-met}}$ is an intermolecular interaction between methanes and is expressed as below:

$$E_{\text{met-met}} = \sum_{\text{pairs}} \frac{1}{4\pi\epsilon} \frac{q_i q_j}{r_{ij}} + \sum_{\text{pairs}} \left\{ \epsilon \left(\frac{r_0}{r_{ij}} \right)^{12} - 2\epsilon \left(\frac{r_0}{r_{ij}} \right)^6 \right\} \quad (5)$$

The fifth energy $E_{\text{met-wat}}$ is an intermolecular interaction between methane and water:

$$\begin{aligned} E_{\text{met-wat}} = & \sum_{\text{pairs}} \frac{1}{4\pi\epsilon_0} \frac{q_i q_j}{r_{ij}} + \sum_{\text{pairs}} \left\{ \epsilon \left(\frac{r_0}{r_{ij}} \right)^{12} - 2\epsilon \left(\frac{r_0}{r_{ij}} \right)^6 \right\} \\ & + \sum_{\text{H-bonds}} \left\{ \epsilon \left(\frac{r_0}{r_{\text{HX}}} \right)^{12} - 2\epsilon \left(\frac{r_0}{r_{\text{HX}}} \right)^{10} \right\} \end{aligned} \quad (6)$$

2.3. Hessian matrix for total potential energy E

The second derivatives $\partial^2 E / \partial q_i \partial q_j$ for the total potential energy E can be summarized with a single equation:

$$\frac{\partial^2 E}{\partial q_i \partial q_j} = (\phi_i, \psi_i) \left\{ s_{ij} \sum_{\xi \in M_i} \sum_{\eta \in M_j} (c_{\xi\eta} C_{ij}^* + d_{\xi\eta} D_{\xi\eta}) \right\} \begin{pmatrix} \phi_j \\ \psi_j \end{pmatrix} \quad (7)$$

Here q_i means the independent variables of each molecule in methane hydrate. The derivation of Eq. (7) is given in Appendix A of Supplementary material.

3. Modelling of methane hydrate

3.1. Two model systems

Compared to the model systems in the previous paper (5^{12} and $5^{12}6^2$), the present work elaborates these models by enclosing them with polyhedra of small and large cages.

First we focussed on the 5^{12} cage and surround with 12 polyhedra consisting of $5^{12}6^2$ cages. This is depicted in Fig. 1(a). In this figure, a central methane (coloured in green) is located at a centre in the 5^{12} cage, which is hereinafter referred to as cage 0, and the other 12 methanes (in red) are located at a centre of each of the 12 large cages, referred to as cages 1–12. Initial configurations of the 13 methanes are constructed by rotating Eulerian angles randomly. The water molecules of the 13 cages are hydrogen bonded to each other. We call this model system with the 5^{12} cage at a centre of the system, an m13 system, and call the 13 methanes in cages 0–12, m0–m12. We see m0 is entirely surrounded by the other methanes, and m1–m12 are partly surrounded.

Next, we surrounded the $5^{12}6^2$ cage with 14 polyhedra consisting of 4 small cages and 10 large cages. This system is depicted in Fig. 1(b), where a central methane in green is at a centre of the $5^{12}6^2$ cage, which is also referred to as cage 0, and 4 small cages surrounding cage 0, referred to as cages 1–4, and the remaining 10 large cages are referred to as cages 5–14. Again the initial configurations of the 15 methanes are created randomly, and appropriate H-bonding networks between waters are constructed. We call this model system with the $5^{12}6^2$ cage at a centre of the model, an m15 system, and call the 15 methanes in cages 0–14, m0–m14. We see m0 is entirely surrounded, and the others are partly surrounded.

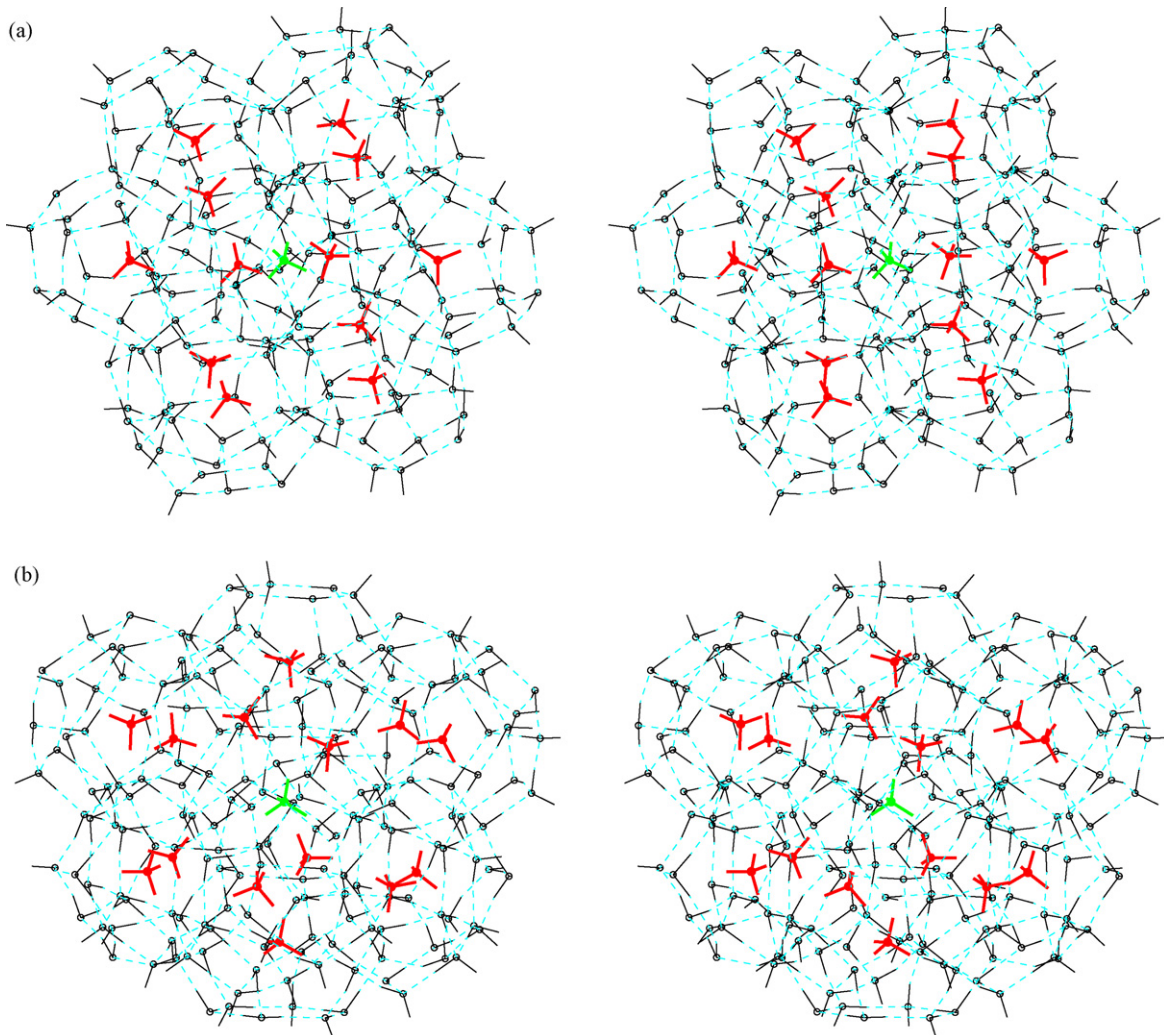


Fig. 1. (a) Stereo view of the 1st network with ran1 configuration for the m13 system. m0 in cage 0 (small cage) is in green and m1–m12 in cages 1–12 (large cage) are in red. Waters are in black and H-bondings are in aqua. (b) Stereo view of the 1st network with ran1 configuration for the m15 system. m0 in cage 0 (large cage) is in green, and m1–m4 in cages 1–4 (small cage) and m5–m14 in cages 5–14 (large cage) are in red.

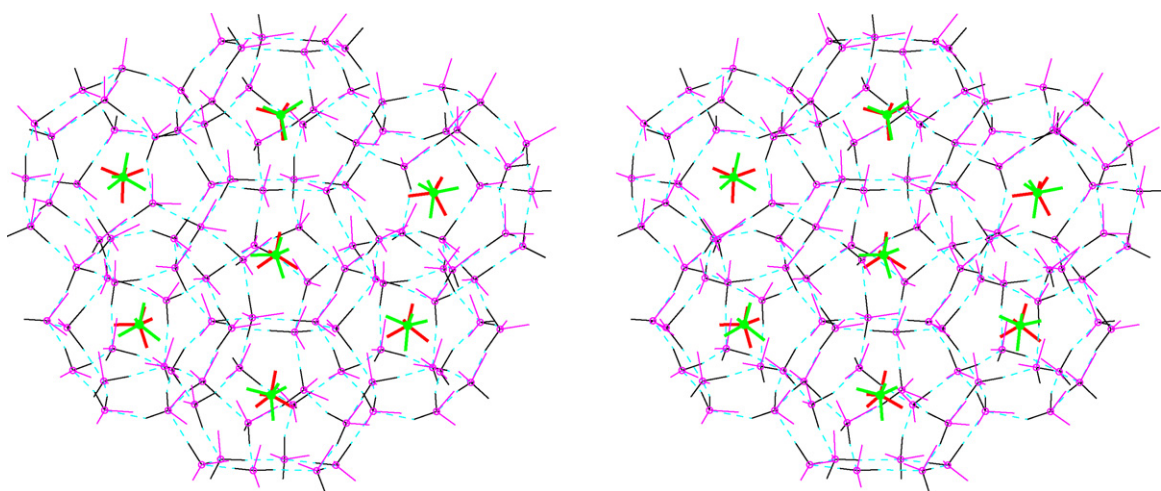


Fig. 2. Stereo view for the m15 system. Waters of the 1st network with methanes (in red) of ran1 configuration are in black, while waters of the 2nd network with methanes (in green) of ran2 configuration are in magenta. For easy perception, only seven cages from among 15 cages are displayed. A central methane of the figure is m0 in cage 0, and the remaining ones are two small cages and four large cages. In addition, hydrogens in the 2nd network deviate a little from the original sites for distinguishing from H-bondings in the 1st network.

3.2. Three hydrogen-bonding networks

As illustrated in Fig. 1(a) and (b), we constructed a proper H-bonding network between water molecules in both the m13 and m15 systems, in addition to the methanes configured randomly in each cage. Hydrogens participating in H-bonding would move forward and backward between two oxygens taking part as donor or acceptor in the H-bonding. Innumerable H-bonding network patterns could be constructed between water molecules. From these patterns, we select a few as follows. Likewise, methanes in hydrate experience innumerable interactions with neighbouring methanes. In order to put methanes in as different environments as possible, we made three different H-bonding network patterns between water molecules both in the m13 and m15 systems, in addition to three different configurations of each methane in the cages. That is, one network pattern of hydrogen bond has three different configurations of methanes. We use the following terminology: in both the m13 and m15 systems, the first H-bonding network pattern (1st network) has three randomly determined initial configurations of methanes (ran1, ran2 and ran3). A 2nd network has also ran1, ran2 and ran3 configurations. A 3rd network has ran1, ran2 and ran3. As an example for the m15 system, we depict in Fig. 2 stereo drawings of the 1st network with ran1 configuration and the 2nd network with ran2 configuration. The combinations of networks and configurations are called assemblies.

4. Results

4.1. Energy minimization both for m13 and m15 systems

Each of the nine assemblies for the m13 system is energy minimized using Newton's method based on a modified Cholesky factorization of the Hessian [9]. Each assembly consists of 13 cages (172 waters) and 13 methanes. The number of degrees of freedom is 1756 { 172×9 and $13 \times (15 + 1)$ }; see Ref. [1]. As in the previous paper, we minimized the total potential energy E of Eq. (1) with the harmonic and anharmonic potential energy in Eq. (4), and with the H-bonding potential between methane and water in Eq. (6). For the H-bonding potential energy between methane and water, we assume the strength to be 75% of the strength between waters. See Refs. [1,10]. Energy minimization is stopped when the energy difference between the current step and the earlier step becomes less than 1.0×10^{-26} aJ. At this point in multidimensional space $\{t_\mu^n, \tau_\mu^n, \rho_v^n, (\mu = 1-3, v = 1-10, n = 0-12), tw_\mu^k, tw_\mu^k, \rho w_v^k, (\mu = 1-3, v = 1-3, k = 1-172)\}$ (see Appendix A of Supplementary material), the subset of the Hessian, whose elements are expressed in terms of t_μ^n (tw_μ^k) and τ_μ^n (tw_μ^k) had six positive eigenvalues for the respective methanes and waters. Likewise the subset expressed in terms of ρ_v^n had 10 positive eigenvalues for the respective methanes. Also the subset expressed in terms of ρw_v^k had three positive eigenvalues for the respective waters.

Similarly, energy minimization was performed on each of the nine assemblies of the m15 system. The system consists of 15 cages (184 waters) and 15 methanes. The number of degrees

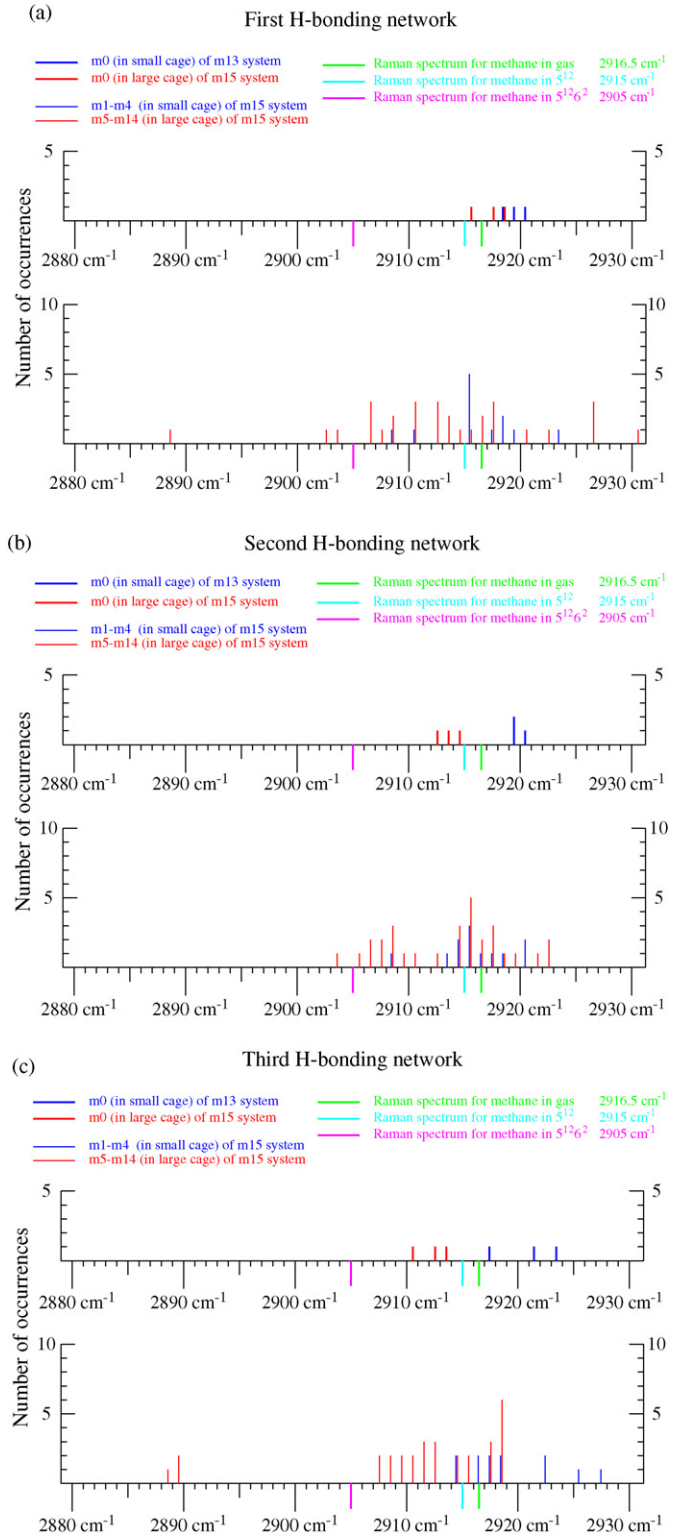


Fig. 3. Histogram of frequency ν_1 of the A1 mode. The frequency is counted as follows: e.g., a frequency ν_1 in the range of $2915.0 \text{ cm}^{-1} \leq \nu_1 < 2916 \text{ cm}^{-1}$ is counted as one at 2915.5 cm^{-1} . The frequencies are in blue for methanes in small cages, and in red for the large. Raman spectra are drawn in green, aqua and magenta. The upper part is provided for methanes in cage 0 with three random orientations for both the m13 and m15 systems, whereas the lower one is for methanes in the cages 1–14 with three random orientations for the m15 system. (a) The 1st network with three random orientations. (b) The 2nd network with three random orientations. (c) The 3rd network with three random orientations.

Table 1

Averaged frequency ν_1 of the A1 mode (in units of cm^{-1})

m13 system	m15 system
m0 (small cage)	2920.0
m1–m12 (large cage)	2912.9
m0 (large cage)	2914.1
m1–m4 (small cage)	2917.2
m5–m14 (large cage)	2912.7

of freedom is 1896 { 184×9 and $15 \times (15 + 1)$ }. We obtained the respective positive eigenvalues for each subset of the Hessian.

4.2. Normal mode analysis of methanes both for m13 and m15 systems

The force constant matrix F necessary to do normal mode analysis is the subset of the Hessian for each methane in the minimum energy configuration, whose elements are

$\partial^2 E / \partial \rho_i^n \partial \rho_j^n$ ($i, j = 1–10$, $n = 0–12$) for the m13 system and ($n = 0–14$) for the m15 system. The kinetic energy matrix G is given in Ref. [1]. Using the symmetry coordinates, these matrices with 10×10 elements are reduced to matrices with 9×9 elements. With the force constant and the kinetic energy matrices, nine normal vibrational frequencies for each methane both in the m13 and m15 systems were obtained. See Ref. [1].

In the calculation of the electrostatic energy between methanes of Eq. (5), we have used $84 \times \varepsilon_0$ for a dielectric constant between methanes. ε_0 is the dielectric constant *in vacuo*. But we realized that some waters forming cages are between methanes and would be more or less tightly bound. So we will use $3 \times \varepsilon_0$ as the dielectric constant instead. To check whether this new dielectric constant affects the nine normal vibrational frequencies of methane, we minimized the model systems studied in Ref. [1], and did normal mode analysis. The numerical values of nine frequencies were the same to the first or second decimal place, e.g., in the 5^{12} cage, 2915.428 cm^{-1}

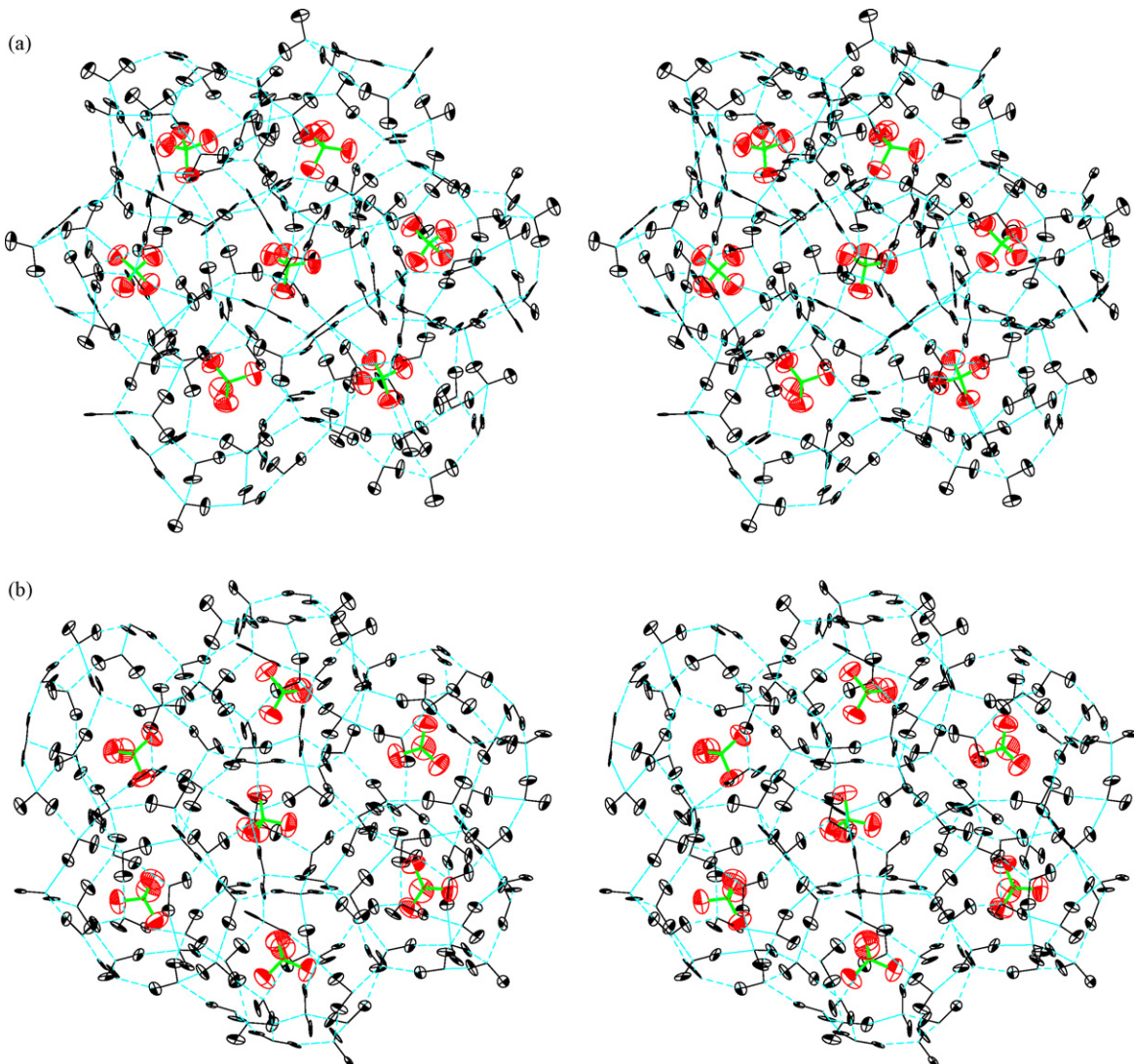


Fig. 4. Stereo view of internal motions of all atoms in the 1st network with ran1 configuration. The thermal ellipsoids of atoms (at 100% probability) are drawn with ORTEP and are magnified 14.42^3 ($=3000$) times for easy recognition. The ellipsoids of carbon and the bonds of methane are in green. Only seven cages for each model system are chosen. (a) For the m13 system. The central methane is m0 in cage 0 (small cage) and the remaining ones are six large cages. (b) For the m15 system. The configuration is the same as Fig. 2.

for $84 \times \varepsilon_0$ and 2915.429 cm^{-1} for $3 \times \varepsilon_0$. Therefore we have perfect confidence in the results reported in our previous paper.

In both the m13 and m15 systems, we minimized the total potential energy with the dielectric constant of $3 \times \varepsilon_0$ and did normal mode analysis of each methane. We focus only on the C–H stretch (A1 mode) frequency ν_1 of each methane. A histogram of frequency ν_1 of the A1 mode is shown in Fig. 3(a) for the 1st network with the three random configurations. The upper histogram of this figure shows for methanes (m0) entirely surrounded by cages the frequencies ν_1 of m0 for the m13 (in blue) and m15 (in red) systems. These three blues are higher than the Raman spectrum 2915 cm^{-1} and the 2916.5 cm^{-1} in gaseous methane. Also in the upper panel three reds are higher than the observed 2905 cm^{-1} and two of the three reds are higher than gaseous methane. On the other hand, the lower histogram shows for m1–m14 of the m15 system the 12 frequencies ν_1 of m1–m4 (in thin blue) for three random configurations in the small cages (cages 1–4) and the 30 frequencies of m5–m14 (in thin red) for three random

configurations in the large cages (cage 5–14). Five of the 12 blues are higher than in gas, while the remaining 7 blues are comparable to 2915 cm^{-1} or lower. Some of the 30 reds are quite high compared to gas, but a few predicted frequencies are lower than 2905 cm^{-1} . On the whole, the frequencies of reds are more widely distributed than the frequencies of blues. Shown respectively in Fig. 3(b) and (c) are histograms of the 2nd network with three random configurations and the 3rd network with three random configurations. Things common to the three histograms are that most blue frequencies of m0 are higher than the 2916.5 cm^{-1} of gas, and most reds of m0 are between 2910 cm^{-1} and 2916.5 cm^{-1} .

In Table 1, we show for small and large cages the calculated frequency ν_1 of the A1 mode, averaged over three H-bonding network patterns with three random configurations. We see that the average value of m1–m12 in the m13 system is comparable to the average of m5–m14 in the m15 system, so we omit analysis of the value of m1–m12 in the m13 system in the following as well as in Fig. 3(a) and (b).

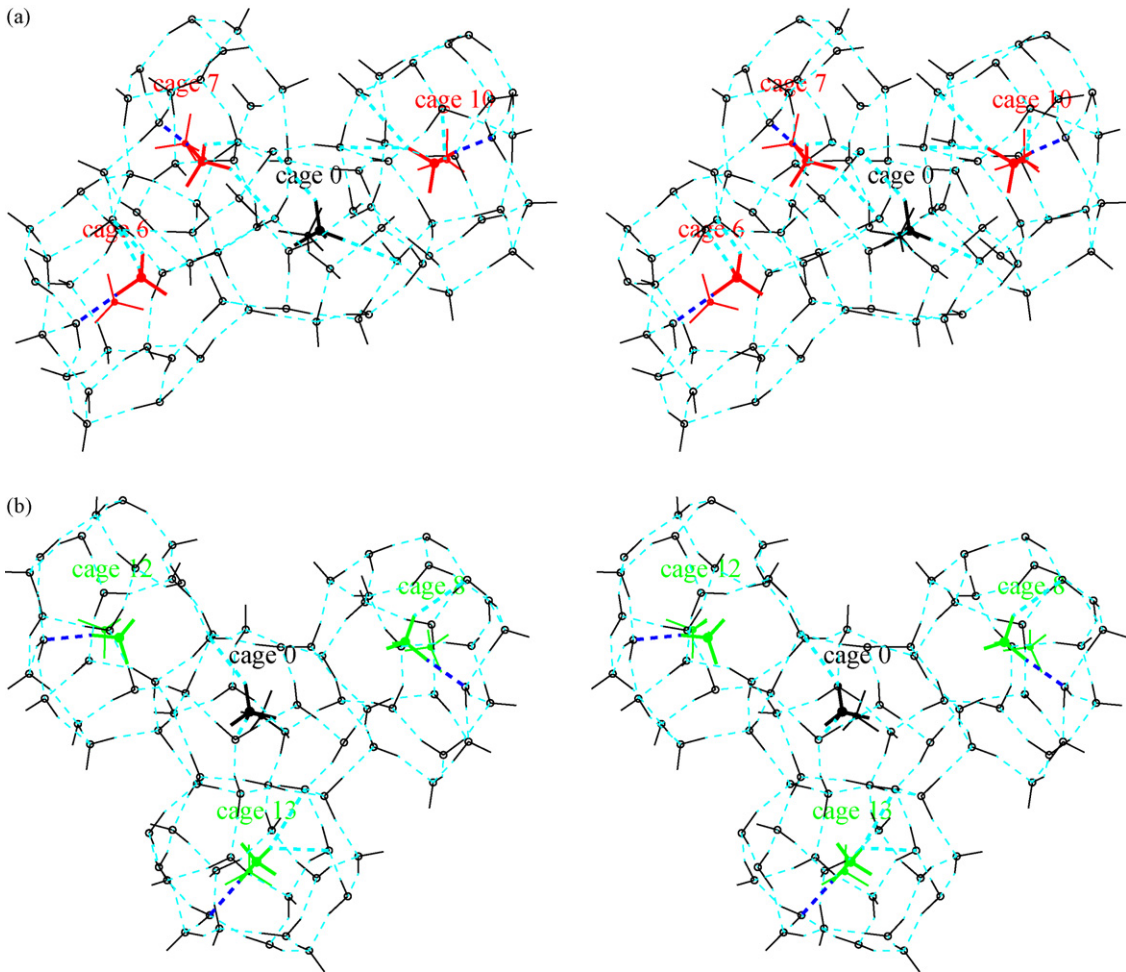


Fig. 5. Stereo view of four cages in the 1st network with ran1 configuration for the m15 system. (a) The methanes with higher frequency are coloured in bold red, i.e., m6 (2922.3 cm^{-1}), m7 (2926.4 cm^{-1}) and m10 (2926.4 cm^{-1}). m0 (2917.4 cm^{-1}) is in black. The methanes in thin red and thin black represent methanes of initial configuration before minimization. The aqua dashed lines exhibit H-bonding between waters. On the other hand, the bold blue dashed lines exhibit H-bondings between methane and water whose separations are less than 2.0 \AA , and the bold aqua dashed lines show those whose distances are between 2.0 \AA and 2.8 \AA . We use the criterion of H-bonding adopted in Ref. [1], i.e., an HM–OW distance must be less than 2.8 \AA , and a CM–HM–OW angle must be larger than 135° . (b) The methanes with lower frequencies are in bold green, i.e., m8 (2908.8 cm^{-1}), m12 (2906.4 cm^{-1}) and m13 (2908.5 cm^{-1}). The methanes in thin green and thin black represent methanes in initial configuration.

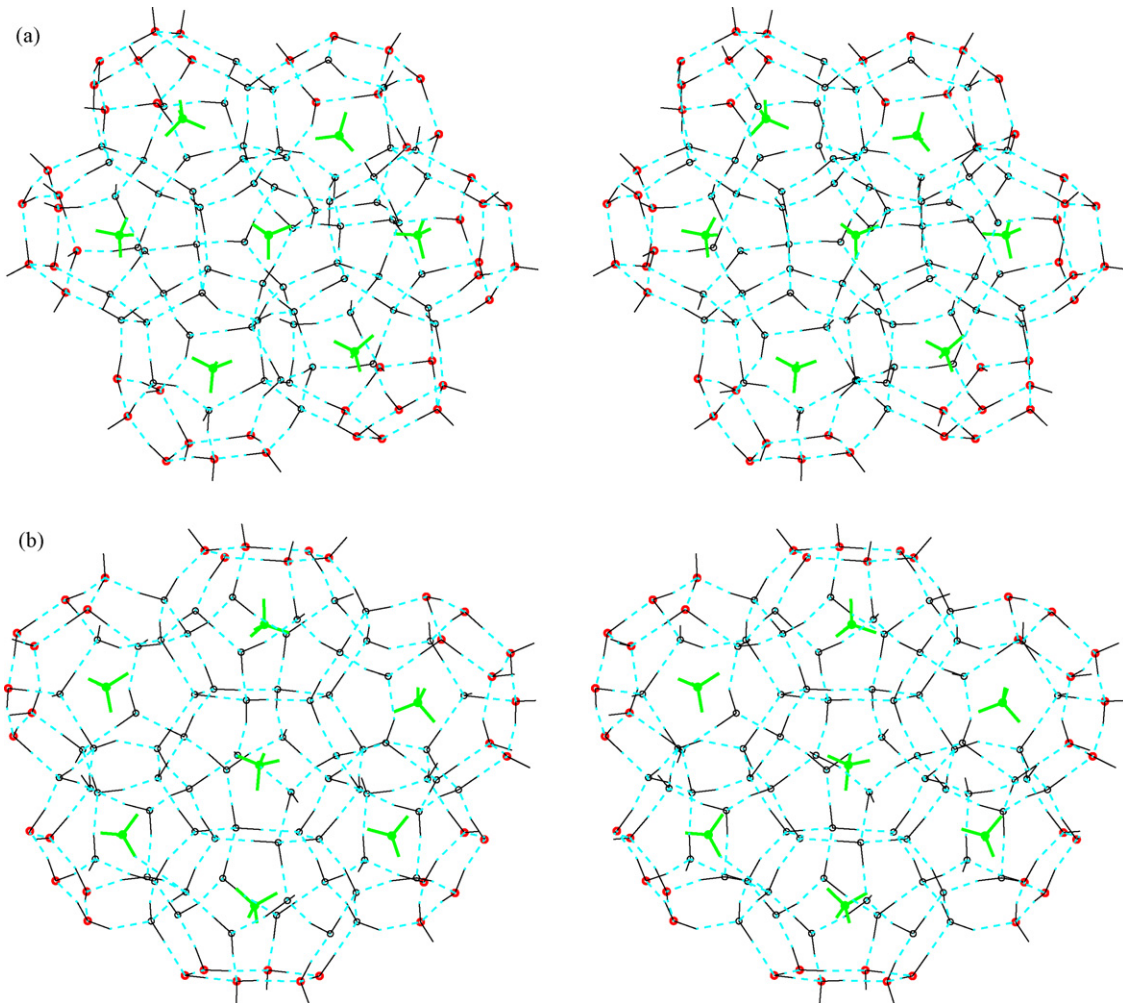


Fig. 6. Stereo view of the model system with surface water fixed. Oxygens of waters on surface of the model system, which are coloured in red, are fixed. (a) For the 2nd network with ran2 configuration in the m13 system. The configuration is the same as Fig. 4(a). (b) For the 3rd network with ran3 configuration in the m15 system. The configuration is the same as Fig. 2 and Fig. 4(b).

With the mean-square displacement matrix including the nine normal vibrational modes, anisotropic thermal vibrations for each methane atom and each water atom in the methane hydrate systems are calculated. See Ref. [1]. We depict the internal motions in the m13 and m15 systems in Fig. 4(a) and (b), respectively [11]. In these figures as well as in subsequent figures, we calculate the displacements that occur when each of the normal modes is thermally excited at 100 K.

5. Discussion and conclusion

5.1. Why we could not get the frequencies ν_1 in agreement with the Raman spectra?

As shown in Table 1, our calculations show that m0 in the small cage of the m13 system has a frequency (2920.0 cm^{-1}) larger than the one (2916.5 cm^{-1}) in gaseous phase. Moreover, a frequency (2914.1 cm^{-1}) of m0 in the large cage of the m15 system is much larger than the Raman spectrum (2905 cm^{-1}) of a large cage. But Table 1 shows that methanes in large cages

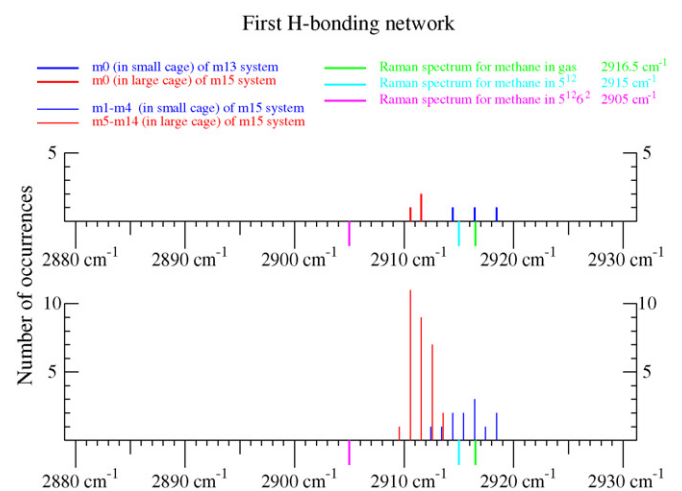


Fig. 7. Histogram of frequency ν_1 of the A1 mode for the 1st network with three random configurations, calculated with the surface water fixed method. The legend is the same as Fig. 3.

have lower frequencies than in small cages, which is the same trend as in the observed Raman spectra. In addition, our calculations show that methane in a cage partly surrounded by other cages, has a lower frequency than the one fully surrounded, for both large and small cages, although this trend has not yet been definitely established experimentally.

To check why the calculated results would not be in good agreement with the Raman spectra, Fig. 5(a) and (b) are provided. In these figures, we choose some cages from those in Fig. 4(b) to delineate outlines of the cages. Fig. 5(a) shows methanes with frequency higher than the Raman spectrum (2905 cm^{-1}) of large cages, while Fig. 5(b) is for methanes with lower frequency. In both figures, we can see that the H-bondings between methane and water, depicted by bold blue dashed lines, deform the cages. We realize that deformed cages

Table 2

Averaged frequency ν_1 of the A1 mode (in units of cm^{-1})

m13 system	m15 system		
m0 (small cage)	2916.6	m0 (large cage)	2911.7
m1–m12 (large cage)	2911.2	m1–m4 (small cage)	2915.9
		m5–m14 (large cage)	2911.3

would raise or lower the frequency of methane. In addition, we realize that such deformed cages could not correspond exactly to the structures found in nature. Thus we have to conclude that the method applied so far to methane hydrate does not suffice. Hence we next suggest a new method where a minimum conformation would model more closely the crystallized structure.

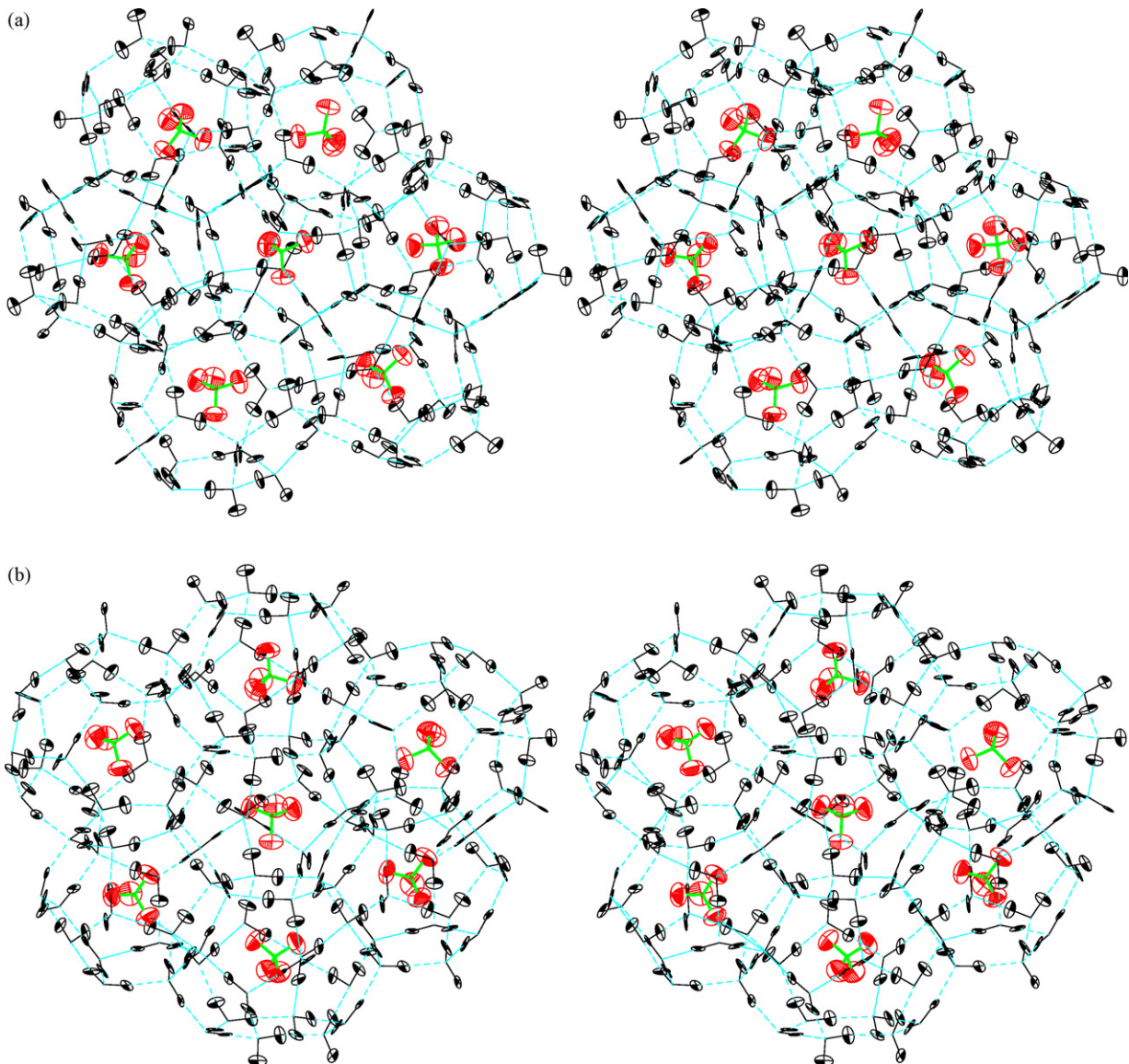


Fig. 8. Stereo view of internal motions of all the atoms, calculated with the surface water fixed method. The thermal ellipsoids of atoms (at 100% probability) are drawn with ORTEP and are magnified 14.42^3 ($=3000$) times for easy recognition. The ellipsoids of carbon and the bonds of methane are in green. (a) For the 2nd network with ran2 configuration in the m13 system. The configuration is the same as Fig. 4(a). (b) For the 3rd network with ran3 configuration in the m15 system. The configuration is the same as Fig. 4(b).

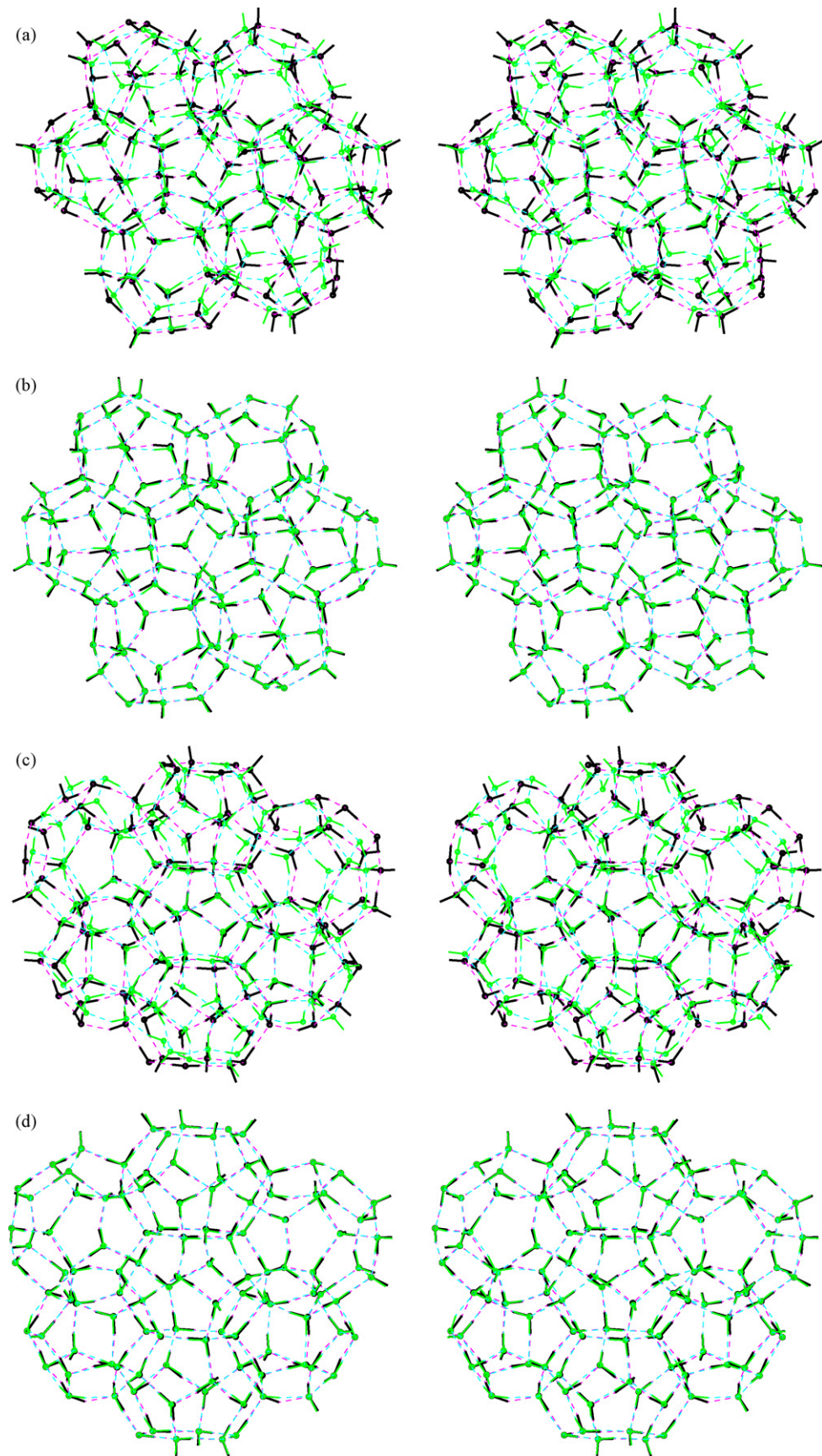


Fig. 9. Stereo view of the model system (in green) best superposed on the X-ray crystallographic structure (in black). (a) For the conformation of the 1st network of Fig. 4(a). The rms deviation of the oxygens from the X-ray structure was 0.758 Å. (b) For the conformation of the 2nd network of Fig. 8(a). The rms deviation was 0.050 Å. (c) For the conformation of the 1st network of Fig. 4(b). The rms deviation was 0.802 Å. (d) For the conformation of the 3rd network of Fig. 8(b). The rms deviation was 0.051 Å.

5.2. A surface water fixed method

An improved method should be based on two characteristics. One of them is that the structure of the methane hydrate must be fitted to the X-ray crystallographic structure. The other is that molecules in the model system should be allowed to move as freely as possible. With these two demands, we offer a new method for treating methane hydrate. As shown in Fig. 6(a) and (b), oxygens more than two oxygens away from any oxygens forming cage 0 are coloured in red. All these red oxygens are fixed. But hydrogens linked to these oxygens can be allowed to move. Waters with oxygens marked in red have three degrees of freedom of Eulerian angles specifying orientation as a rigid-body motion of water and three degrees of freedom of internal motions. The other waters and all methanes are allowed to move freely as done in the energy minimization so far. We call this new method a surface water fixed method. In this method, the dielectric constant between methanes is set to ϵ_0 .

Again, we minimized the total potential energy of each of the nine assemblies of three H-bonding network patterns with three random methane orientations in both the m13 and m15 systems. At the energy minimum point, six positive eigenvalues for each subset of the Hessian expressed in terms of variables of a rigid-body motion for the respective methanes and waters could not be obtained because of the constraints on the fixed waters. But we could get 10 positive eigenvalues of the respective methanes, and three positive eigenvalues of the respective waters for each subset of the Hessian expressed in terms of internal variables. Hence we could do normal mode analysis of each methane and of each water.

In Fig. 7, we show a histogram of frequency ν_1 of the A1 mode for the 1st network with three random configurations. We omit histograms for the 2nd and 3rd networks because a similar trend is shown in their histograms. Also in Table 2, we give for the small and large cages the calculated frequency ν_1 of the A1 mode, averaged over three H-bonding network patterns with three random configurations. We see that all the values shown in Table 2 are lower than the corresponding values in Table 1, calculated by the minimization with no constraints. Now the frequency (2916.6 cm^{-1}) of m0 in the small cage is almost the same as the one (2916.5 cm^{-1}) in gas, and moreover we can see that the difference (4.9 cm^{-1}) between the frequency of m0 in the small cage and of m0 in the large cage is comparable with the corresponding difference (5.9 cm^{-1}) shown in Table 1. As a result, we can say that the frequencies calculated by the new method are a little nearer to the Raman spectra than the ones calculated by the method with no constraints. We depict the internal motions of methanes and waters in the 2nd network with ran2 configuration for the m13 system in Fig. 8(a), and also depict the motions in the 3rd network with ran3 configuration for the m15 system in Fig. 8(b).

Comparing Fig. 8(a) with Fig. 4(a) for the m13 system, we see that the structures of cages in Fig. 8(a) are almost retained at the X-ray crystallographic structure. To show this quantitatively, Fig. 9(a) and (b) are provided. Fig. 9(b) shows that the conformation of cages fits nicely on the X-ray structure, while the conformation minimized with no constraints has a

comparatively large rms deviation from the X-ray structure (i.e., 0.758 \AA for oxygen). We can say the same thing for Fig. 8(b) and Fig. 4(b) of the m15 system. Fig. 9(c) and (d) are also provided to show quantitatively.

In this subsection, we have discussed results calculated by the surface water fixed method and results from the method with no constraints. The treatments we have done so far can be considered to be extremes, i.e., one in which waters on the surface are fixed, and the other is that all waters are allowed to be free, except for the constraints of H-bonding. We might think it would be valuable to try a method between these extremes. We do so in the next subsection.

5.3. A middle method

We might expect that if the fixed waters on the surface can be allowed to move gradually, we could get results close to experiment. To test this expectation, we allow surface oxygens (coloured in red in Fig. 6(a) and (b)) to move within a volume of radius $r (\text{\AA})$, whose centre is at a fixed point. With this model, we minimized the total potential energy of each of the nine assemblies of three H-bonding network patterns with three

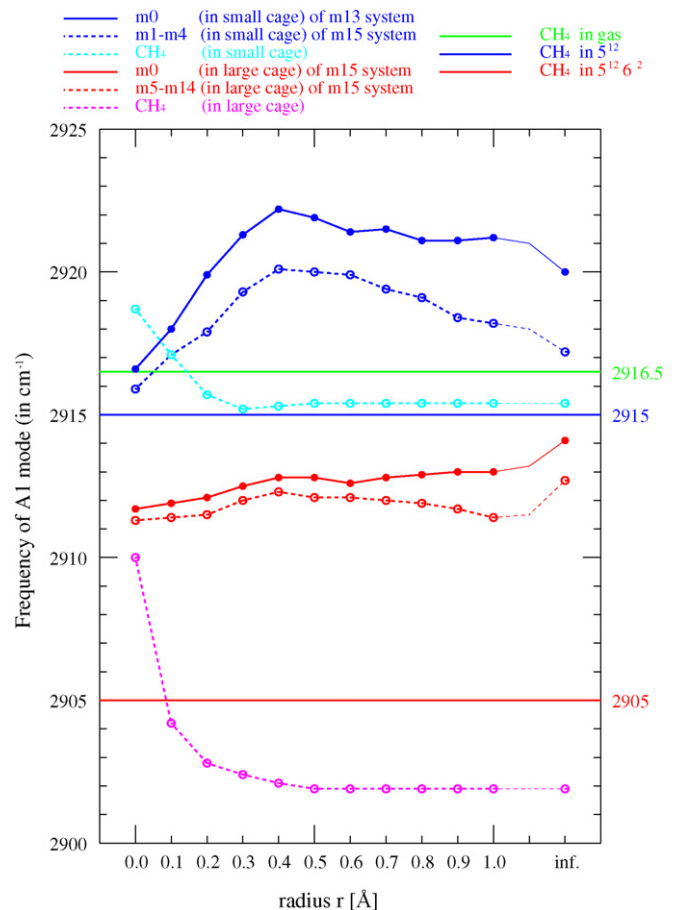


Fig. 10. Frequency ν_1 of the A1 mode are plotted against the radius $r (\text{\AA})$ of oxygen movement. The blue lines indicate the frequencies of the small cage, whereas the red lines indicate the large cage. The green line shows the frequency in gaseous methane. The aqua line represents the frequency of the small cage adopted in Ref. [1], whereas the magenta line represents the large cage.

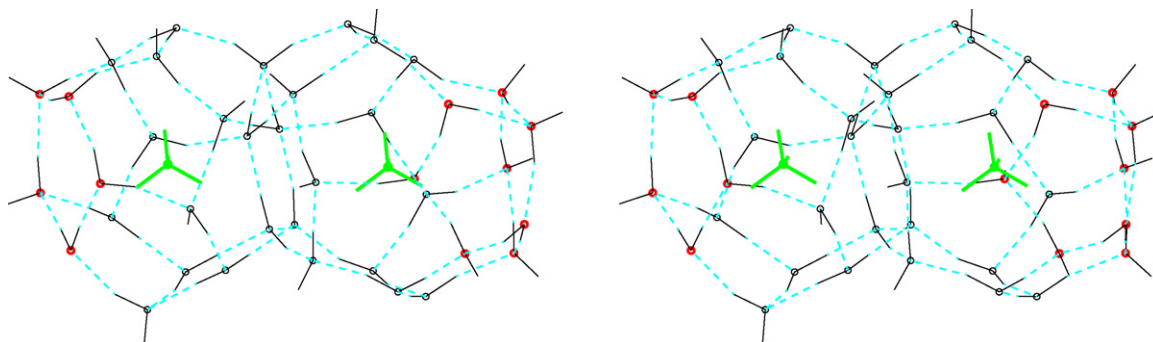


Fig. 11. Stereo view of the two cages model system adopted in Ref. [1], with surface water fixed. Oxygens separated by more than two oxygens from any oxygens forming the pentagon shared by two cages are coloured red, and those all oxygens are fixed.

random orientations for the m13 and m15 systems. In Fig. 10, we show for small and large cages the frequency ν_1 of the A1 mode, averaged over three H-bonding network patterns with three random configurations plotted against the radius r (\AA) parameter. Frequencies calculated at radius 0.0 \AA are values given in Table 2. Frequencies are calculated up to radius 1.0 \AA . Frequencies at infinite (inf.) radius are values obtained by the method with no constraints and are the ones in Table 1. At a glance, we see that frequencies at radius 0.0 \AA for both the small and large cages are the lowest. The frequencies for both size cages increase up to a radius 0.4 \AA ; beyond that the frequencies for the small cage are going down more or less to the values at infinite radius, whereas the frequencies for the large cage are going up more or less to the values at infinite radius. The results in Fig. 10 suggest that frequencies at radius 0.0 \AA are in best agreement with the observed Raman spectra.

Also in Fig. 10, we give the frequency ν_1 for the small and large cages in the two cages model system adopted in Ref. [1]. In this calculation, fixed oxygens on the surface of the model system are illustrated in Fig. 11. Frequencies at infinite radius are values (2915.4 cm^{-1} , 2901.9 cm^{-1}) obtained in Ref. [1]. From Fig. 10, we see that frequencies at radius 0.0 \AA for both cages are the highest, and then the frequencies decline to the values at infinite radius. This trend is contrary to that for the larger model systems adopted in the present article. Why do the trend differ? We see from Fig. 11 that the methanes in the both cages are subject to interactions with the fixed oxygens. We would think these methanes might be feeling stiffer because of the fixed waters; hence these methanes would have higher frequencies. We could guess that as the radius of oxygen movement expands, the methanes would feel softer to other atoms, and then the methanes would have lower frequencies. However, let us look at Fig. 6(a) and (b). Methanes in cage 0 in both systems undergo interactions with the flexible oxygens, not from the fixed oxygens. These methanes would be feeling loose from the flexible waters, and then these would have lower frequencies. Again looking at Fig. 11, we might think that the methane in the large cage would feel only weak potentials from the fixed oxygens, and so the methane would be in an environment similar to the methanes in large cages depicted in Fig. 6(b). Therefore the frequencies estimated at radius 0.0 \AA coloured in red and magenta of Fig. 10 are not so different.

In summary, we could say that Fig. 10 describes two things. From the frequencies coloured in blue and red, if an energy minimum conformation of the model system would be fitted to the X-ray crystallographic structure, we could get the lowest frequencies in both small and large cages. On the other hand, from the frequencies coloured in aqua and magenta, if the waters are allowed to move freely, we would also get lower frequencies. At first glance, these two things seem likely to contradict each other. But from the above two points of view, it would be possible to reduce frequencies in both small and large cages. That is, if we constructed a model system vastly larger than the model system used in this article, and if the oxygens of surface waters of the model system were fixed, it would follow that the inner methanes could move freely, such as in nature. We are now planning research in that direction.

In conclusion, we have described a new method called the surface water fixed method in this article. With this method, the frequencies calculated at radius 0.0 \AA for small and large cages are in moderate agreement with the Raman spectra, though not entirely satisfactorily. The model systems analysed almost reproduce the X-ray crystallized structure. By constructing a model system larger than the present models, it should be possible to obtain frequencies in good agreement to the Raman spectra. All the analytical results presented here are obtained using the energy parameters adopted in Ref. [1], except for the dielectric constant between methanes. Again we would say it is necessary to use the cubic anharmonic potential energy within methane and to use the H-bonding potential energy between methane and water, whose strength is 75% of the strength of H-bonding potential between waters. With the independent molecule model, dynamical structures of methane hydrates will be even more thoroughly studied in future.

Appendix A. Supplementary data

Supplementary data associated with this article can be found, in the online version, at doi:10.1016/j.jmgm.2008.01.005.

References

- [1] S. Yoshioki, Application of the independent molecule model to elucidate the dynamics of structure I methane hydrate, J. Mol. Graphics Modell. 25 (2007) 856–869.

- [2] E.D. Sloan Jr., Clathrate Hydrates of Natural Gases, 2nd ed., Marcel Dekker Inc., New York, 1998 (Revised and expanded).
- [3] R.K. McMullan, G.A. Jeffrey, Polyhedral clathrate hydrates. IX. Structure of ethylene oxide hydrate, *J. Chem. Phys.* 42 (1965) 2725–2732.
- [4] A.K. Sum, R.C. Burruss, E.D. Sloan Jr., Measurement of clathrate hydrates via Raman spectroscopy, *J. Phys. Chem. B* 101 (1997) 7371–7377.
- [5] L.-M. Chou, A. Sharma, R.C. Burruss, J. Shu, H. Mao, R.J. Hemley, A.F. Goncharov, L.A. Stern, S.H. Kirby, Transformations in methane hydrates, *Proc. Natl. Acad. Sci. U.S.A.* 97 (2000) 13484–13487.
- [6] T. Uchida, R. Okabe, K. Gohara, S. Mae, Y. Seo, H. Lee, S. Takeya, J. Nagao, T. Ebinuma, H. Naria, Raman spectroscopic observations of methane-hydrate formation and hydrophobic hydration around methane molecules in solution, *Can. J. Phys.* 81 (2003) 359–366.
- [7] D.L. Gray, A.G. Robiette, The anharmonic force field and equilibrium structure of methane, *Mol. Phys.* 37 (1979) 1901–1920.
- [8] W.T. Raynes, P. Lazzaretti, R. Zanasi, A.J. Sadlej, P.W. Fowler, Calculations of the force field of the methane molecule, *Mol. Phys.* 60 (1987) 509–525.
- [9] P.E. Gill, W. Murray, M.H. Wright, Practical Optimization, Academic Press, London, 1981, p. 105.
- [10] T. Ida, M. Mizuno, K. Endo, Electronic state of small and large cavities for methane hydrate, *J. Comput. Chem.* 23 (2002) 1071–1075.
- [11] C.K. Johnson, ORTEP: A Fortran Thermal Ellipsoid Plot Program, ORNL-3795, Oak Ridge National Laboratory, Oak Ridge, Tennessee, USA, 1965.
- [12] S. Yoshioki, Formulation of the Hessian matrix for the conformational energy of protein-water systems, *J. Phys. Soc. Jpn.* 66 (1997) 2927–2935.